LIMNOLOGY and OCEANOGRAPHY: METHODS

Headwater gas exchange quantified from O_2 mass balances at the reach scale

L. Rovelli [ID],[1,2]* K. M. Attard [ID],[2,3] C. M. Heppell,[4] A. Binley,[5] M. Trimmer,[6] R. N. Glud[2,7]
[1]Scottish Marine Institute, Scottish Association for Marine Sciences, Oban, United Kingdom
[2]Nordcee, Department of Biology, University of Southern Denmark, Odense M, Denmark
[3]Tvärminne Zoological Station, University of Helsinki, Hanko, Finland
[4]School of Geography, Queen Mary University of London, London, United Kingdom
[5]Lancaster Environment Centre, Lancaster University, Lancaster, United Kingdom
[6]The School of Biological and Chemical Sciences, Queen Mary University of London, London, United Kingdom
[7]Department of Ocean and Environmental Sciences, Tokyo University of Marine Science and Technology, Tokyo, Japan

Abstract

Headwater streams are important in the carbon cycle and there is a need to better parametrize and quantify exchange of carbon-relevant gases. Thus, we characterized variability in the gas exchange coefficient (k_2) and dissolved oxygen (O_2) gas transfer velocity (k) in two lowland headwaters of the River Avon (UK). The traditional one-station open-water method was complemented by in situ quantification of riverine sources and sinks of O_2 (i.e., groundwater inflow, photosynthesis, and respiration in both the water column and benthic compartment) enabling direct hourly estimates of k_2 at the reach–scale (~ 150 m) without relying on the nighttime regression method. Obtained k_2 values ranged from 0.001 h^{-1} to 0.600 h^{-1}. Average daytime k_2 were a factor two higher than values at night, likely due to diel changes in water temperature and wind. Temperature contributed up to 46% of the variability in k on an hourly scale, but clustering temperature incrementally strengthened the statistical relationship. Our analysis suggested that k variability is aligned with dominant temperature trends rather than with short-term changes. Similarly, wind correlation with k increased when clustering wind speeds in increments correspondent with dominant variations (1 $m\ s^{-1}$). Time scale is thus an important consideration when resolving physical drivers of gas exchange. Mean estimates of k_{600} from recent parametrizations proposed for upscaling, when applied to the settings of this study, were found to be in agreement with our independent O_2 budget assessment (within < 10%), adding further support to the validity of upscaling efforts aiming at quantifying large-scale riverine gas emissions.

Revisions of the global carbon cycle have indicated that rivers and other inland waters contribute substantially to the global cycling of organic carbon and emission of carbon dioxide (CO_2) and methane (CH_4) to the atmosphere (e.g., Cole et al. 2007; Battin et al. 2008; Tranvik et al. 2009; Aufdenkampe et al. 2011; Raymond et al. 2013; Hotchkiss et al. 2015; Stanley et al. 2015; Marx et al. 2017). However, due to a lack of an appropriate universal scaling for quantification of emissions, headwaters (stream order < 4) were initially not included in these assessments (*see* Cole et al. 2007), despite the fact they

represent 17% of global riverine area (in perennial riverine systems e.g., Downing et al. 2012). Later inclusions of headwaters have proposed that small streams (order 1) might represent more than a third of the total regional emissions of CO_2 from riverine systems (Butman and Raymond 2011) and thus could be more prominent at the global scale (Raymond et al. 2013). This has highlighted the need for better constraining gas exchange at the reach scale (Trimmer et al. 2012), with the overarching goal of fine-tuning parametrizations used for large scale and global upscaling of metabolism and gas emissions.

Accurate assessments of gas exchange require quantification of the gas transfer velocity, or piston velocity (k; unit of length per unit of $time^{-1}$, e.g., $m\ h^{-1}$), which physically controls the exchange of gases at the stream–air interface (*see* Hall et al. 2012). Thus, estimates of k are critical to the assessment of emission of greenhouse gases such as CO_2 (e.g., Hotchkiss et al. 2015; Marx et al. 2017) and CH_4 (e.g., Stanley et al. 2015; Crawford and Stanley 2016) and for the quantification

*Correspondence: lorenzo@biology.sdu.dk

Additional Supporting Information may be found in the online version of this article.

of the gas exchange rate of dissolved oxygen (O_2) and estimates of whole-reach metabolism (e.g., Odum 1956). Stream gas exchange is most commonly assessed from total, i.e., whole-stream, metabolism estimates using open water (OW) methods based on local dissolved oxygen (O_2) mass balances (e.g., Odum 1956; Marzolf et al. 1994; Mulholland et al. 2001; Riley and Dodds 2013; Siders et al. 2017). The OW approach provides an integrative quantification of gas exchange R_{ex} (in μmol L^{-1} unit of $time^{-1}$) as

$$R_{ex} = k_2 \left(O_{2(sat)} - O_2 \right) \tag{1}$$

with ($O_{2(sat)}$ - O_2) being the O_2 saturation deficit, i.e., the difference between the O_2 concentration at saturation for the local physical conditions ($O_{2(sat)}$) and the actual O_2 concentration in the stream water, and k_2 the O_2 gas exchange coefficient, often termed the re-aeration coefficient (k_2 or K, unit of $time^{-1}$, e.g., h^{-1}). The coefficient k_2 represents the product of the depth-corrected O_2 gas transfer velocity, or piston velocity (k; unit of length per unit of $time^{-1}$, e.g., m h^{-1}) and local stream area-to-volume ratio, which is often approximated as the inverse of the mean water depth (in m^{-1}) (*see* Raymond et al. 2012; Demars et al. 2015). As assessments of gas exchange critically rely on the quantification of k_2 or k, several direct and indirect methods have been developed for deriving these values.

Direct measurements of these parameters are characterized by the de-gassing of a conservative tracer gas that is subsequently scaled to O_2 (e.g., Wanninkhof et al. 1990; Genereux and Hemond 1992; Reid et al. 2007; Benson et al. 2014). This approach is logistically demanding and temporal upscaling is difficult (Demars et al. 2015). Indirect measurements depend on parameterizations of the local physical characteristics of the stream reach such as depth, flow and slope (e.g., Parker and Gay 1987; Parker and DeSimone 1992 and references therein), as well as fitting of gas transfer parameters to O_2 time series based on simplified relationships (Hornberger and Kelly 1975; Chapra and DiToro 1991; McBride and Chapra 2005) or more complex modeling efforts (Holtgrieve et al. 2010; Grace et al. 2015; Appling et al. 2018). Empirical equations and parameterizations have proven to be useful as predictors of gas-exchange dynamics for specific reaches (*see* Genereux and Hemond 1992), but usually show large discrepancies in k_2 estimates when applied to streams with comparable hydrological characteristics (Moog and Jirka 1998; Aristegi et al. 2009; Palumbo and Brown 2014). To further constrain these parametrizations for spatial upscaling, recent studies have focused on a better characterization of the stream morphology. For example, Raymond et al. (2012) used a large collection of stream metadata to more rigorously scale k parametrizations to stream physical characteristics (i.e., flow, depth, slope, discharge).

Although k variability on short timescales, i.e., hours, has been reported (e.g., Tobias et al. 2009; Berg and Pace 2017), direct and indirect methods mostly focus on determining a mean value for k_2 for either the day or night, or an average for the whole day-night period, with little consideration being given to its short-term dynamics that are characteristic of most rivers. Recent application of the aquatic eddy co-variance technique (AEC) in rivers has provided robust assessment of reach-scale (~ 150 m) benthic metabolism (Koopmans and Berg 2015; Rovelli et al. 2017) and, most recently, an "inverted" AEC approach has been used to directly quantify O_2 gas exchange in large (order 3) streams (Berg and Pace 2017) and in an estuarine embayment (Long and Nicholson 2018). Yet, irrespective of the approach being applied to assess k, little emphasis has been given to small headwaters streams (order 1–2), despite their potential implications for the regional and global carbon cycling (e.g., Butman and Raymond 2011; Raymond et al. 2013).

The goal of our study was to provide a proof-of-concept for the derivation (values and dynamics) of k_2 and k at the reach scale in small, headwater streams (stream order 1). This was achieved by combining in situ O_2 measurements from a single station OW approach together with direct assessments of riverine metabolism using AEC, sample incubations, and groundwater inflow measurements. The proposed method was compared to the traditional nighttime regression (NR) method, and was used to characterize temporal variability in k on hourly to daily time scales. Furthermore, we evaluate k dynamics and its relation to the local physical drivers such as mean stream flow, temperature and wind patterns. The results of this study are discussed in light of parametrizations of k for regional to large-scale upscaling.

Materials and procedures

Study site

This study focused on two headwaters of the Hampshire River Avon, southern England: the Chalk River Ebble (CE) and the Greensand West Avon (GA) (*see* Heppell et al. 2017; Supporting Information Fig. S1). For each headwater, a representative ~ 150 m reach was selected based on previous surveys of the sub-catchment morphology and geology (*see* "Field measurements" section). The selected CE reach (CE1[1]; 51° 1′ 41.171″ N/1° 54′ 56.309″ W) was investigated over 3 d (25–27 April 2013) in spring, when the reach was characterized by a net outflow of stream water to the aquifer, i.e., a losing reach (*see* Supporting Information Fig. S2). The reach was also characterized by profuse growth (36% cover by area) of *Ranunculus* spp., which is widespread throughout the sub-catchment (Watson 1987). The water column of the River Ebble was characterized by low turbidity, with suspended sediment concentration limited to, on average, 37 mg L^{-1} (Heppell and Binley 2016*a*). The selected GA reach (GA2; 51° 19′ 10.173″ N/1° 51′ 33.135″ W) was investigated over 3 d from 28–30 April 2013. In contrast to the CE reach, the GA reach was characterized by a constant inflow of low-oxygenated groundwater; i.e., a gaining reach (Supporting Information Fig. S2) and only patchy

---

[1] Reach designations within the Macronutrient Cycles Programme (https://nerc.ukri.org/research/funded/programmes/macronutrient/).

macrophyte coverage (4% by area). Turbidity in the water column was 40% higher on average than at the CE reach (Heppell and Binley 2016*a*). The reaches are referred to as CE and GA throughout the text.

Reach scale oxygen budget

The assessment of O_2 gas exchange and stream metabolism based on a single station open-water approach (e.g., Odum 1956) relies on O_2 time series. Temporal changes in O_2 concentration, dO_2/dt, are attributed to local whole-stream primary production (P), respiration (R) and atmospheric exchange (R_{ex}) as

$$\frac{dO_2}{dt} = P + R + R_{ex} = P + R + k_2\left(O_{2(sat)} - O_2\right) \quad (2)$$

with k_2 being the gas exchange coefficient (in h^{-1}) and ($O_{2(sat)} - O_2$) the O_2 saturation deficit. The spatial integration of a one-station approach, i.e., the integrated stretch length along the stream, is typically in the order of 1000s of m and can be quantify as $3v/k_2$, with v being the mean stream flow velocity (in m d^{-1}) and k_2 (in d^{-1}) (*see* Grace and Imberger 2006).

Rates for R and R_{ex} are typically estimated by applying the established nighttime regression (NR) method (Hornberger and Kelly 1975). The method plots the nighttime dO_2/dt at each time step against the O_2 saturation deficit during the night and assumes $P = 0$ and that respiration is light-independent. The resulting linear relationship, obtained via least-squares regression, provides both k_2 (slope) and R (intercept). As NR-based k_2, k_{NR}, is only obtained at night, many studies have adopted a temperature correction term to account for temperature changes between night and day following the parameterization of Elmore and West (1961):

$$k_{2(T)} = k_{2(20°C)}(1.0241)^{(T-20)} \quad (3)$$

where $k_{2(20°C)}$ is the gas exchange coefficient at 20°C and $k_{2(T)}$ the gas exchange coefficient at the given temperature T.

The O_2 budget (OB) approach used in the current study expands Eq. 2 by accounting for all relevant processes including (1) metabolic activity in both sediment and water, and (2) exchange with both the atmosphere and groundwater (Fig. 1). The temporal O_2 concentration was thus defined as:

$$\frac{dO_2}{dt} = \frac{A}{V}[F_B + F_{WC} + F_K] \quad (4)$$

where F_B, F_{WC}, F_K are the O_2 flux (in mmol m^{-2} h^{-1}) associated with the benthic compartment, the water column, and atmospheric exchange, respectively. The O_2 fluxes were expressed as volumetric rates (in μmol L^{-1} h^{-1}) by multiplying the values by the average ratio between stream area (A) and stream volume (V), which, under smooth stream water surface
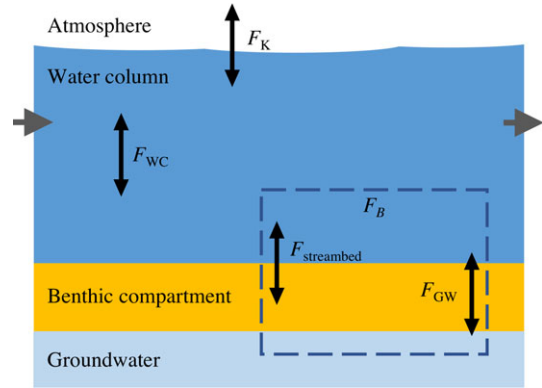
Fig. 1. Dissolved oxygen mass balance approach. Changes in stream O_2 concentration are expressed as a function of contributions from the water column (F_B), benthic compartment (F_B), and atmospheric exchange (F_K) following the parameterization of Eq. 4. Benthic F_B includes contributions from the streambed ($F_{streambed}$) and from groundwater inflow/outflow (F_{GW}). Note that lateral exchange and advection processes were not considered.

conditions, is approximated as the mean stream depth (d) (Demars et al. 2015).

The main strength of the proposed approach is that each flux component within the OB (Eq. 4) can be directly quantified in the field. Estimates of F_B were obtained from aquatic eddy co-variance (AEC) measurements, while F_{WC} was quantified by incubating discrete water samples in situ (*see* "Field measurements" section). While F_B does include both streambed ($F_{streambed}$) and groundwater contributions to the O_2 budget, fluxes associated with the inflow of O_2 depleted groundwater were independently quantified as:

$$F_{GW} = v_{gw}\left(O_{2(gw)} - O_2\right) \quad (5)$$

with $O_{2(gw)}$ being the groundwater O_2 concentration (in μmol L^{-1}), O_2 the in-stream concentration and v_{gw} the local groundwater inflow (in m h^{-1}).

The atmospheric exchange rate was quantified as:

$$F_K = \frac{V}{A}k_2\left(O_{2(sat)} - O_2\right) \quad (6)$$

with $k = k_2(V/A) \approx k_2d$ being the O_2 gas transfer velocity, or O_2 piston velocity (in m h^{-1}) and $O_{2(sat)}$ the local O_2 concentration at saturation. As $O_{2(sat)}$ can be quantified as a function of temperature (*see* Garcia and Gordon 1992), the OB approach effectively enabled a direct estimate of k_2.

To facilitate comparisons with published reference values and parameterizations from previous studies, k_2 values were also expressed as $k_{2(20°C)}$ (*see* Eq. 3). Similarly, estimates of O_2 gas transfer velocity were also standardized to a Schmidt number of 600[2] (k_{600}) based on Jahne et al. (1987) as

---

[2] Schmidt number for CO_2 at 20°C and O_2 at 17.5°C in freshwater.

$$\frac{k_{600}}{k} = \left(\frac{600}{Sc_T}\right)^{-1/2} \qquad (7)$$

where $Sc_T \approx 0.00086842T^4 - 0.10115T^3 + 4.8055T^2 - 124.34 T + 1745.1$ is the Schmidt number for O_2 in freshwater at the local water temperature T (*see* Wanninkhof 2014). Stream temperature time series were obtained from background measurements of physical parameters during the observational period at each site (Rovelli et al. 2016*b*).

Field measurements

Site selection

The investigated reaches (CE and GA) were carefully selected to represent the sub-catchment dominant stream morphology features (e.g., stream course shape, depth, bends, riparian zone) and in-stream habitat patchiness (macrophytes, sediment type). Particular emphasis was given to ensure that each reach also fulfilled the theoretical requirements of the NR method, i.e., streams with relatively high metabolic activity and low gas exchange (*see* Hornberger and Kelly 1975). Field measurements were also executed under stable hydrological condition, i.e., constant flow and mean water depth over ≥ 3 d. This enabled (1) the evaluation of our local O_2 budget (OB) method and (2) comparisons with the nighttime regression (NR) method and standardized functional equations for k_2 quantification from mean hydrological parameters.

Background physicochemical measurements

Stream water column O_2 concentration, temperature, and photosynthetically active radiation (PAR) at the streambed (~ 15 cm above the bottom) were monitored within each reach at 1 min intervals with a conductivity–temperature–depth logger (CTD; XR-420, RBR, Kanata, Canada), equipped with an Aanderraa O_2 optode sensor (Aanderaa, Bergen, Norway) and a 4π PAR sensor (QCP-2000; Biospherical Instruments, San Diego, U.S.). The data were also used to calibrate the O_2 sensors used for flux estimates and to define nighttime periods (PAR < 2 μmol quanta m^{-2} s^{-1}). Wind speed and direction near the stream surface (1.5 m elevation) were recorded at 15 s intervals with a SkyWatch GEOS 11 portable weather station (JDC Electronic SA, Yverdon-les-Bains, Switzerland).

Benthic oxygen flux

The benthic oxygen flux was quantified using the AEC technique (Berg et al. 2003). Our AEC module consisted of small, lightweight, stainless steel tripod frame equipped with an acoustic Doppler velocimeter (ADV; Vector, Nortek A/S, Rud, Norway), Clark-type O_2 microelectrodes (Revsbech 1989), and submersible O_2 amperometric amplifiers (McGinnis et al. 2011). Up to two O_2 microelectrodes were positioned ~ 0.5 cm outside the ADV sampling volume, at an inclination of ~ 60°. Each microelectrode had a 90% response times < 0.5 s and stirring sensitivity < 0.5% (Gundersen et al. 1998). The ADV's flow measurements were obtained at 8–15 cm from the streambed with a frequency of 64 Hz and with the ADV x-axis aligned to the main flow direction. The acquired datasets were processed following the same procedure described in Rovelli et al. (2017). In short, the dataset was averaged to 8 Hz while applying data quality controls and despiking routines (e.g., Mori et al. 2007) to the dataset to remove dataset artifacts and reduce signal noise. A double coordinate rotation was applied to the flow time series to minimize the influence of horizontal motions on the vertical velocity component. The datasets were then aligned, i.e., time-shifted, to account for the relative distance between the ADV sampling volume and the microelectrode tip and for the microelectrode time constant (*see* Donis et al. 2015). The AEC-based turbulent oxygen fluxes (in mmol m^{-2} h^{-1}) were estimated from time-averaged vertical velocity fluctuations (w') and O_2 concentration fluctuations (C'), as

$$F_{AEC} = \overline{w'C'} \qquad (8)$$

(*see* Berg et al. 2003) via a Reynolds' decomposition, specifically linear detrending, using the program suite Sulfide-Oxygen-Heat Flux Eddy Analysis (SOHFEA version 2.0; *see* McGinnis et al. 2014). The optimal detrending interval represents a trade-off between including low-frequency turbulent contributions and excluding non-turbulent contributions (McGinnis et al. 2008), and was inferred to be 5 min from cumulative averages of oxygen fluxes and friction velocity (u_*) (*see* Attard et al. 2014). To account for the effect of transient O_2 concentration changes in the water column between the sediment–water interface and the AEC measurement height (h), which can potentially bias F_{AEC} (*see* Holtappels et al. 2013; Rheuban et al. 2014), an O_2 storage term was estimated after Rheuban et al. (2014). The benthic oxygen flux corrected for O_2 storage, F_B, was defined as

$$F_B = F_{AEC} + F_{storage} = F_{AEC} + \int_0^h \frac{dC}{dt}dz \qquad (9)$$

with dC/dt being the measured O_2 concentration gradient.

The smallest area of the streambed that contributes to 90% of AEC flux, termed the "footprint area", was estimated from the sediment surface roughness parameter (z_0) and h following the parameterization by Berg et al. (2007). Values for z_0 were approximated as $z_0 = h \cdot \exp\left(-\kappa \cdot \frac{u}{u_*}\right)$ with κ being the von Karman constant (0.41), and u the average flow velocity (Wüest and Lorke 2003).

Water column activity

Water column oxygen production and consumption rates were estimated by incubating 100 mL rack-mounted glass bottles in situ over 24 h in the light and in the dark, with continuous measurements of O_2 concentration via O_2 optical fibers (4 channel FirestingO2; Pyro Science GmbH, Aachen,

Table 1. Summary of hydrological and physicochemical data for river Ebble (CE) and West Avon (GA). Average values are presented as mean ± standard error. Values between square brackets indicate the range of the measurements.

Site	Period	Daylight [h]	Daily PAR [mol m^{-2} d^{-1}]	O_2 [% sat]	O_2 [μmol L^{-1}]	T [°C]	Depth[a] [m]	Width[a] [m]	Flow [m s^{-1}]	Discharge[a] [m^3 s^{-1}]
CE	25–27 Apr 2013	15.3	11.9	106.6±0.3 [87.7–132.7]	367.7±0.9 [301.5–449.5]	10.8±0.03 [8.4–13.5]	0.41	5.25	0.18	0.640
GA	28–30 Apr 2013	15.3	17.4	101.5±0.3 [82.3–127.2]	365.3±1.2 [303.0–449.3]	9.0±0.02 [7.8–10.7]	0.57	2.75	0.33	0.385

[a]Obtained from depth and flow velocity transects performed during the observational period under stable hydrograph (*see* Rovelli et al. 2016*a*).

Germany). A set of one dark bottle, and one clear bottle were incubated at the streambed, while one bottle was incubated near the stream surface. The fourth bottle was either incubated at mid-depth at GA (depth > 0.4 m) or near the surface for the shallower CE. Three additional replicate sets were also mounted on the rack but O_2 measurements were only performed at the start and end of each incubation via Winkler titrations (Winkler 1888). Volumetric oxygen fluxes (in μmol L^{-1} h^{-1}) were estimated from temporal O_2 concentration gradients via linear regressions for daytime and nighttime periods, respectively. No difference in fluxes were observed at the different depths, indicating a homogenously, well-irradiated water column and thus depth-independent rates. The areal oxygen fluxes F_{WC} (in mmol m^{-2} h^{-1}) were obtained by multiplying the values with the average stream depth. Contributions from macrophytes were deemed to be well-integrated within benthic measurements and thus were not further addressed within the water column oxygen budget (Rovelli et al. 2017).

Groundwater influx

Dissolved oxygen flux resulting from local inflow of O_2 depleted groundwater was estimated based on measurements of the local hydraulic gradients from in-stream piezometers and porewater O_2 concentrations. Two clusters of in-stream piezometers were installed at each site, ~ 10 m apart in the river thalweg. Each cluster comprised three piezometers screened at 20 cm, 50 cm, and 100 cm depth; the 100 cm piezometer was also fitted with narrow polytetrafluoroethylene tubing to depths of 10 cm, 20 cm, 30 cm, 50 cm, 70 cm, and 100 cm for the purposes of pore water sampling. Installation and design of the piezometers followed the description in Binley et al. (2013).

Hydraulic head was measured in all piezometers using HOBO pressure transducers (Onset Computer Corporation, Bourne, U.S.) at GA and Levelogger Edge pressure transducers (Solinst, Georgetown, Canada) at CE. Measurements were validated with manual dips on a fortnightly basis and, if needed, corrected assuming a linear drift. River stage was measured using a pressure transducer suspended within a stilling well. Falling and rising head slug tests (measurements taken by pressure transducers installed inside the piezometers) were used for computation of saturated hydraulic conductivity using the Hvorslev method

(e.g., Binley et al. 2013). Vertical groundwater flux was computed using Darcy's Law, from measurements of the hydraulic gradient between the 50 cm deep piezometric head and local stream stage, combined with a weighted harmonic mean of hydraulic conductivity from slug tests carried out in the 20 cm and 50 cm deep piezometers (*see* Binley et al. 2013).

Pore water samples were collected from sampling tubes located on the piezometers every 2 months, from February 2014 to June 2016, using a syringe and tygon tubing. The O_2 concentration of pore water and river water was measured immediately following sample collection using a calibrated Clark-type O_2 microelectrode (50 μm tip) connected to an in-line amplifier and data-logging meter (Unisense, Aarhus, Denmark) (*see* Heppell and Binley 2016*b*).

Data handling

Collected hydrological and physicochemical data were used to (1) characterize average conditions at each reach and (2) assess short term, i.e., hourly, to diel dynamics. O_2 fluxes obtained for each stream compartment were considered separately, to assess their magnitude and variability within and across the reaches, as well as within the O_2 budget context, to quantify and characterize k variability.

## Assessment

Reach characterization

Hydrological data and background information for each reach are summarized in Table 1. Temperature ranged from 7.8°C to 13.5°C overall, reflecting a moderate variation (< 5%) between day and night at the two sites. Daily integrated PAR (PAR$_{24}$) ranged between 11.9 mol quanta m^{-2} d^{-1} and 17.4 mol quanta m^{-2} d^{-1}, with peaks of up to 1630 μmol quanta m^{-2} s^{-1}. Overall, the average stream flow, based on ADV measurements (12 cm above the streambed), was in the order of 0.18–0.33 m s^{-1} with an associated discharge of 0.209–0.640 m^3 s^{-1} (Table 1) and showed no significant change between day and night, or within the observational period, indicating a stable flow. Wind speeds at CE showed irregular patterns but an overall higher wind speed during the day than at night (Fig. 2). Wind dynamics at GA, in contrast, were markedly diel, with an average wind speed of 2.4–3 m s^{-1} during the day and 0–0.2 m s^{-1} at night (Fig. 3).

At both sites the water column showed well-defined diel fluctuations in O_2 concentration, with nighttime under-saturation (down to 82%) and daytime oversaturation (up to 133%), with diel O_2 concentration changes reaching ∼ 147 μmol L^{-1} (Figs. 2–3). The O_2 saturation deficit ranged from −108 to −96 μmol L^{-1} during the day, to 43–65 μmol L^{-1} at night. The average deficit over 24 h ranged from 2 μmol L^{-1} to an O_2 saturation surplus of 15 μmol L^{-1}.

Dissolved oxygen budget

Benthic compartment

Hourly oxygen fluxes for the benthic compartment ranged between −14.0 mmol m^{-2} h^{-1} and 23.0 mmol m^{-2} h^{-1} (Figs. 2–3). At CE, oxygen fluxes followed a clear diel pattern (Fig. 2), with average daytime rates of 4.2 mmol m^{-2} h^{-1} and nighttime rates of −2.8 mmol m^{-2} h^{-1}. AEC-based benthic
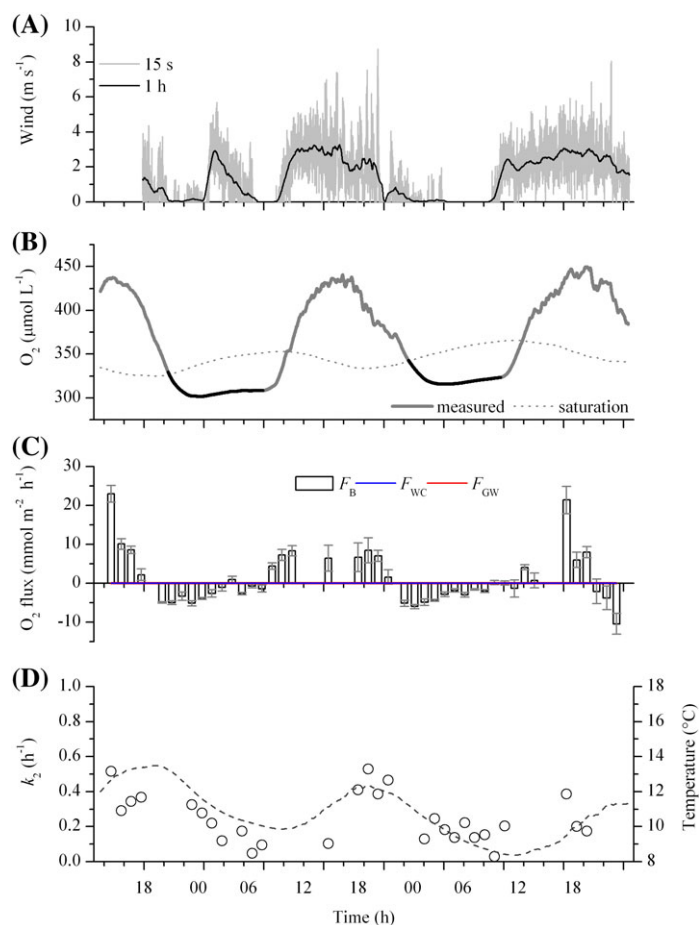
Fig. 2. Estimates of k_2 for the River Ebble (CE) during the spring. (**A**) Wind speed recorded 1.5 m above the stream surface. (**B**) Local dissolved oxygen (O_2) concentration (gray line) and associated O_2 concentration at atmospheric saturation (dotted line). Black lines indicate nighttime (PAR < 2 μmol quanta m^{-2} s^{-1}). (**C**) Time series of oxygen fluxes encompassing benthic (F_B), water column (F_{WC}), and groundwater (F_{GW}) contributions to the local O_2 budget. (**D**) Hourly averaged estimates of k_2 based on the O_2 budget (OB) method in spring (circles), with temperature overlain (dashed line).
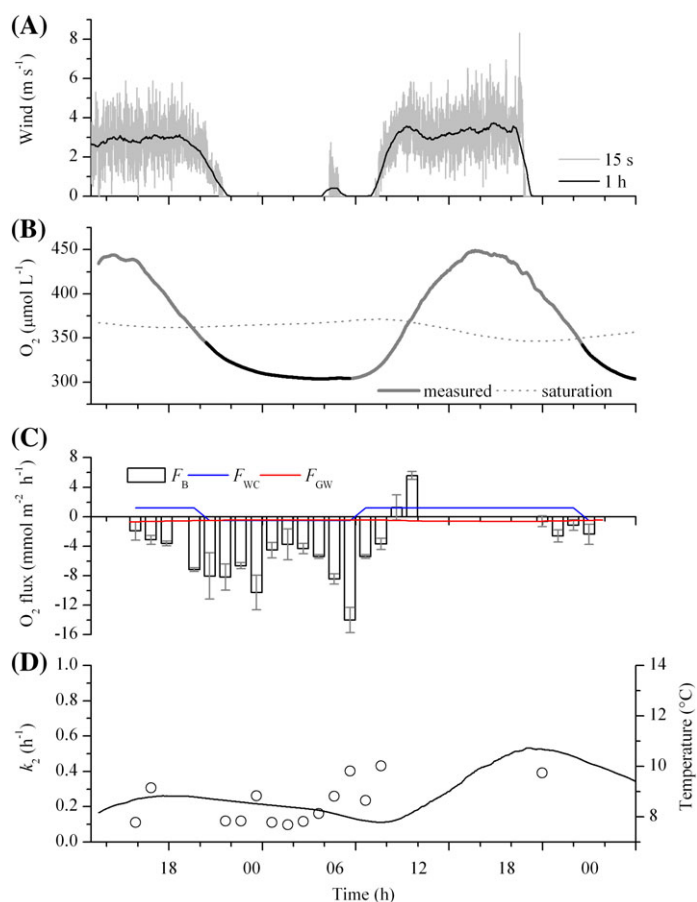
Fig. 3. Estimates of k_2 for the river West Avon (GA) during the spring. (**A**) Wind speed recorded 1.5 m above the stream surface. (**B**) Local dissolved oxygen (O_2) concentration (gray line) and associated O_2 concentration at atmospheric saturation (dotted line). Black lines indicate nighttime (PAR < 2 μmol quanta m^{-2} s^{-1}). (**C**) Time series of oxygen fluxes encompassing benthic (F_B), water column (F_{WC}), and groundwater (F_{GW}) contributions to the local O_2 budget. (**D**) Hourly averaged estimates of k_2 based on the O_2 budget (OB) method in spring (circles), with temperature overlain (solid line). Note that the wind data were shifted by 24 h to fill the measurement gap on day 1.

fluxes were estimated to cover a footprint area 26 m long and 1 m wide (∼ 20 m^2), with most of the flux contribution, i.e., the region of maximum flux, located 0.5 m upstream of the AEC sampling point. At GA, a diel pattern in the benthic oxygen fluxes was also observed (Fig. 3). However, both mean fluxes at night and during the day were negative, amounting to −6.2 mmol m^{-2} h^{-1} and −3.0 mmol m^{-2} h^{-1}, respectively. The theoretical footprint area was 80 m long and 1 m wide (∼ 70 m^2) with the region of maximum flux located 2 m upstream of the of the AEC sampling point.

Water column

At CE, metabolic activity in the water column was below detection (< 0.1 μmol L^{-1} h^{-1}) and negligible for the local O_2 budget (Fig. 2). In contrast, in the more turbid, sandy GA, water

column activity ranged from net oxygen production rates of 2.8 μmol L^{-1} h^{-1} during the day, to oxygen consumption of -0.9 μmol L^{-1} h^{-1} at night. The average daytime rate of oxygen production was ~ 1.2 mmol m^{-2} h^{-1}, with an average nighttime consumption rate of -0.5 mmol m^{-2} h^{-1} (Fig. 3).

Groundwater

During our study, the CE reach was losing water to the aquifer. This net local outflow of stream water had no measurable effect on in-stream O_2 concentrations (Fig. 2). At gaining reach GA, the inflow of groundwater amounted to 0.043 m d^{-1} on average, with a mean groundwater O_2 concentration of 63.5 μmol L^{-1}. Groundwater contributed to an areal O_2 concentration decrease of -0.4 mmol m^{-2} h^{-1} to -0.7 mmol m^{-2} h^{-1} (average -0.5 mmol m^{-2} h^{-1}), representing 6–7% of the combined nighttime flux caused by metabolic activity in the benthic compartment and the water column (Fig. 3).

Atmospheric exchange

The derived rate of O_2 exchange between the stream and the atmosphere ranged from -22.3 mmol m^{-2} h^{-1} to 14.5 mmol m^{-2} h^{-1}. Estimates of k_2 based on the O_2 budget (OB) method ranged from 0.001 to 0.600 h^{-1}, with mean values of 0.252 h^{-1} and 0.259 h^{-1} for CE and GA, respectively (Table 2). Within such range of k_2 and with mean flow velocities of 0.18–0.33 m s^{-1}, one-station based assessment are expected to integrate a stream length of > 7 km).

Estimates of the gas exchange coefficient k_2 using the NR method (k_{NR}) were 0.555 h^{-1} at CE and 0.434 h^{-1} at GA (Table 3; Supporting Information Fig. S3), and thus around a factor 2 higher than those obtained with the OB method. (Tables 2–3). At CE, we observed a significant ($p < 0.01$) difference between daytime and nighttime estimates of k_2 (Fig. 2; Table 2). The average daytime k_2 (k_{day}) was 0.331 h^{-1} and about 2 times higher than k_2 at night (k_{night}). Similar conditions were observed at GA (Fig. 3; Table 2), suggesting that diel

Table 2. Estimates of k_2 (in h^{-1}) using the O_2 budget (OB) method. Values for daytime, nighttime, and average over the observational period are reported as mean $\pm$ standard error, with n indicating the number of averaged data points. Standardized $k_{2(20°C)}$ (in h^{-1}) and k_{600} (in m h^{-1}) are also reported to enable better comparisons with literature studies.

Site	Day	Night	Mean
		k_2 [h^{-1}] (n)	
CE	0.331$\pm$0.024 (63)	0.170$\pm$0.012 (62)	0.252$\pm$0.015 (125)
GA	0.367$\pm$0.034 (26)	0.188$\pm$0.020 (37)	0.261$\pm$0.021 (63)
		$k_{2(20°C)}$ [h^{-1}] (n)	
CE	0.404$\pm$0.030 (63)	0.214$\pm$0.014 (62)	0.310$\pm$0.019 (125)
GA	0.478$\pm$0.045 (26)	0.248$\pm$0.027 (37)	0.343$\pm$0.028 (63)
		k_{600} [m h^{-1}] (n)	
CE	0.157$\pm$0.012 (63)	0.084$\pm$0.006 (62)	0.121$\pm$0.007 (125)
GA	0.265$\pm$0.025 (26)	0.137$\pm$0.015 (37)	0.190$\pm$0.016 (63)

changes in temperature and wind could partly explain the observed difference between day and night variability in k_2 at both sites.

Dynamics and variability of O_2 gas exchange
Temperature

Gas exchange coefficient (k_2) and gas transfer velocity (k) are expected to be related to local stream temperature (Elmore and West 1961; Kilpatrick et al. 1989; Demars and Manson 2013). Yet, temperature has been reported to be a weak predictor of k in some settings (Tobias et al. 2009; Demars and Manson 2013), as well as in modeling studies (e.g., Correa-Gonzalez et al. 2014). For example, Tobias et al. (2009) used a modified sulfur hexafluoride (SF$_6$) tracer approach to assess variability in k (k_{SF6}) on time scales of hours (in 3 h intervals) and found that k_{SF6} varied by 30% over a 32 h observational period and could apportion 39% of the observed variability to changes in temperature (Demars and Manson 2013).

At CE, our hourly estimates of k varied by 60%, on average, between consecutive measurements during our 3 d observational period, with temperature accounting for 46% of that variability (Supporting Information Fig. S4). As expected from previous studies (e.g., Tobias et al. 2009; Demars and Manson 2013), part of this variability could be accounted for by applying the Elmore and West (1961) temperature correction to normalize k to 20°C (k_{20}; Supporting Information Fig. S4). However, we found that temperature corrected k_{20} could only explain 10% of the k–temperature relationship, and only 5% of the variability measured in k at CE. This provided further evidence that the dynamics of k could not be properly accounted for by simple functions for temperature corrections.

Instead, at CE we found that the relationship between k and temperature could be strengthened by clustering k values to fixed temperature increments, increasing stepwise from 0.5°C to 1.7°C. The best linear relationships (i.e., highest regression coefficients) were observed by clustering data in increments of 1.0–1.5°C ($R^2 > 0.8$), with R^2 decreasing, either side, for shorter or longer increments (Supporting Information Fig. S4) and we found the best fit to the data occurred with 1.5°C increments (Fig. 4A). As the clustering procedure partially accounts for the variability in both temperature and k, the trend in increasing fit to the data (higher R^2) suggested that dynamics in k and temperature, and their interaction, may occur at variable time scales. This trend was, however, not observed at GA, where temperature revealed no direct correlation with k on hourly time scales ($R^2 = 0.02$) or with temperature clustering ($R^2 = 0.03$), indicating that temperature changes in the water column did not significantly contribute to k variability at the site.

Temperature dynamics, however, may affect gas exchange without any detectable changes in bulk O_2 concentrations in the water, as recently proposed by Berg and Pace (2017). The authors applied the same AEC approach as in this study, but in an "upside-down" configuration, with

Table 3. Estimates of k_2 using the nighttime regression method (k_{NR}). Values are reported with the respective regression coefficient (R^2) for each site. The associated plots are available in the Supporting Information (Fig. 3). The temperature-normalized values of k_{NR} for 20°C ($k_{NR(20°C)}$), are computed based on the mean nighttime temperature at each site, while the daily NR-based k scaled for a Schmidt number of 600 ($k_{NR(600)}$, in m h^{-1}) was computed for the mean daily temperatures.

Site	k_{NR} [h^{-1}] (R^2)	$k_{NR(20°C)}$ [h^{-1}]	$k_{NR(600)}$ [m h^{-1}]	Night temperature (°C)
CE	0.554 (0.78)	0.694	0.273	10.5
GA	0.421 (0.78)	0.539	0.304	8.7

AEC measurements being performed near the (underside) of the stream surface (~ 5 cm below the atmosphere–water interface), rather than near the streambed. This enabled the quantification of O_2 flux and heat flux across the stream surface, from which they inferred local O_2 gas exchange and values for k. Their results showed that temperature fluctuations occurring just below the surface might bias the quantification of O_2 fluctuations and thus AEC-based assessments of k. The implications of the study by Berg and Pace (2017) suggest that other methodological approaches commonly used for the quantification of k at timescales ranging from minutes to complete diel cycles could also be impacted. The absence of any relationship between water column temperature and k at GA could thus, in part, be attributed to small-scale temperature dynamics that are not accounted for by simple temperature correction functions; although other physical parameters such as wind, for example, could also modulate k at GA.

Wind

Here the reaches were open to the wind (e.g., Supporting Information Fig. S1), with frequent wind-induced ripples being observed during the day, suggesting an interaction between flow and wind that could affect gas exchange. On time scales of hours, however, wind dynamics revealed no significant relationship with the derived variability in k ($R^2 = 0.13$). Similar results have also been reported from other methodological approaches, e.g., tracer release (Tobias et al. 2009) and AEC (Berg et al. 2017); although both studies relied on off-site, rather than on-site wind measurements. As large variability in both k and wind might mask any general trend, wind data were temporally clustered to investigate any time lag between wind dynamics and derived k values. Using a bin interval of 1 m s^{-1}, which represented the dominant (> 90%) wind fluctuations at each site (Supporting Information Fig. S5), we revealed a robust positive linear relationship ($R^2 > 0.7$) between local wind and k_{600} at each site and for both sites combined (Fig. 4B). Given the relatively low range in wind speed (0–4 m s^{-1}), a linear relationship provided a suitable approximation, although for more extensive ranges in wind speed a quadratic form is more appropriate (e.g., Wanninkhof 1992; Nightingale et al. 2000; Sweeney et al. 2007; Wanninkhof 2014). Similarly to the effect of temperature, increasing or decreasing the size of the wind clustering increment resulted in a lowering of the regression coefficient, thus further supporting the argument of a temporal misalignment between the drivers of k variability and actual k dynamics.

Discussion

Parametrization of gas exchange coefficients

Our study was performed under stable discharge and constant stream depth, which allowed both (1) the evaluation of our local O_2 budget (OB) method for deriving k_2 directly and then, (2) the comparison with the nighttime regression (NR) method and standardized functional equations for k_2 quantification (Table 4). The advantage of the OB method over the latter approaches is that the method is not limited to stable hydrological conditions or specific time periods. This

Fig. 4. Temperature and wind dependencies of the gas transfer velocity k. (**A**) Temperature relationship of k at CE. Values for k (solid black circles), k normalized to 20°C (k_{20}; open gray circles) and to a Schmidt number of 600 (k_{600}, solid gray circles) were clustered into 1.5°C temperature increments to account for temporal misalignments and to provide the most robust linear analysis ($R^2 > 0.9$; *see* Supporting Information Fig. S4). (**B**) Standardized k_{600} as a function of wind speed for CE (solid black squares), GA (open white squares) and both sites combined (dotted line). Wind speeds were clustered into 1 m s^{-1} bins to account for the dominant magnitude of wind fluctuations (*see* Supporting Information Fig. S5). Linear trends were obtained via least squares regression.

Table 4. Estimates of k_{600} (in m h^{-1}) from established empirical equations applied to the CE and GA study sites. Input variables[a]: d, stream depth (m); u, flow velocity (m s^{-1}); u^*, friction velocity (m s^{-1}); s, stream slope (m m^{-1}); Q, discharge (m^3 s^{-1}); and $Fr = u/\sqrt{gd}$, Froude number with g being the gravitational acceleration constant. Note that most equations provide k_2 at 20°C ($k_{2(20°C)}$, in day^{-1}; Supporting Information Table S1); $k_{2(20°C)}$ values that were scaled to k_{600} based on Eq. 7 and the O₂ Schmidt number for 20°C (Table 1).

Eq.	Reference	Abbr.[b]	Equations	CE k_{600} [m h^{-1}]	GA
1	O'Connor and Dobbins (1958)	OD	$k_{2(20°C)} = 3.9\frac{u^{0.5}}{d^{1.5}}$	0.099	0.114
2a	Churchill et al. (1962)	E$_4$	$k_{2(20°C)} = 0.0217\frac{u^{2.695}}{d^{3.085}s^{0.825}}$	0.009	0.023
2b		CEB	$k_{2(20°C)} = 5.01\frac{u^{0.969}}{d^{1.673}}$	0.067	0.096
3	Krenkel and Orlob (1963)	E$_6$, KO	$k_{2(20°C)} = 173.01\frac{(us)^{0.404}}{d^{0.66}}$	0.199	0.285
4a	Owens et al. (1964)	E$_8$	$k_{2(20°C)} = 6.91\frac{u^{0.73}}{d^{1.75}}$	0.148	0.180
4b		E$_9$, OEG	$k_{2(20°C)} = 5.35\frac{u^{0.67}}{d^{1.85}}$	0.139	0.158
5	Dobbins (1965)	DB[e]	$k_{2(20°C)} = 55.2\frac{1+Fr^2}{(0.9+Fr)^{1.5}}\frac{(us)^{0.375}}{d}\coth\left[\frac{4.75(us)^{0.125}}{(0.9+Fr)^{0.5}}\right]$	0.117	0.139
6a	Langbein and Durum (1967)	E$_7$	$k_{2(20°C)} = 5.14\frac{u}{d^{1.33}}$	0.048	0.078
6b		LD	$k_{2(20°C)} = 5.14\frac{u}{d^{0.67}}$	0.026	0.054
7	Issacs and Gaudy (1968)	IG	$k_{2(20°C)} = 4.76\frac{u}{d^{1.5}}$	0.051	0.080
8	Cadwallader and McDonnell (1969)	E$_3$, CM	$k_{2(20°C)} = 186.07\frac{(us)^{0.5}}{d}$	0.136	0.184
9	Negulescu and Rojanski (1969)	NR	$k_{2(20°C)} = 10.91\left(\frac{u}{d}\right)^{0.85}$	0.085	0.150
10	Thackston and Krenkel (1969)	TK[e]	$k_{2(20°C)} = 24.9\frac{u^*(1+Fr^{0.5})}{d}$	0.013	0.025
11	Padden and Gloyna (1971)	PG	$k_{2(20°C)} = 4.53\frac{u^{0.703}}{d^{1.054}}$	0.055	0.082
12a	Bennett and Rathbun (1972)	E$_1$, BR1	$k_{2(20°C)} = 32.69\frac{u^{0.413}s^{0.273}}{d^{1.408}}$	0.163	0.183
12b		E$_2$, BR2	$k_{2(20°C)} = 5.58\frac{u^{0.607}}{d^{1.689}}$	0.140	0.161
13	Parkhurst and Pomeroy (1972)	PP[e]	$k_{2(20°C)} = 48.5\frac{(1+0.17Fr^2)(us)^{0.375}}{d}$	0.097	0.122
14	Bansal (1973)	BN	$k_{2(20°C)} = 1.81\frac{u^{0.6}}{d^{1.4}}$	0.036	0.045
15	Owens (1974)	–	$k_{2(20°C)} = 50.8\frac{u^{0.67}}{d^{0.85}}$[c]	0.236	0.373
16	Tsivoglou and Neal (1976)	E$_{10}$, TN	$k_{2(20°C)} = k_2' us$[d]	0.128	0.325
17	Smoot (1988)	SM	$k_{2(20°C)} = 543\frac{u^{0.5325}s^{0.6236}}{d^{0.7258}}$	0.136	0.206
18	Thackston and Dawson (2001)	TD[e]	$k_{2(20°C)} = 4.97\frac{u^*(1+9Fr^{0.25})}{d}$	0.012	0.024
19a	Raymond et al. (2012)	Rm$_1$	$k_{600} = 5037(us)^{0.89}d^{0.54}$	0.113	0.231
19b		Rm$_2$	$k_{600} = 5937(1-2.54Fr^2)(us)^{0.89}d^{0.58}$	0.125	0.252
19c		Rm$_3$	$k_{600} = 1162u^{0.85}s^{0.77}$	0.096	0.160
19d		Rm$_4$	$k_{600} = 951.5(us)^{0.76}$	0.097	0.154
19e		Rm$_5$	$k_{600} = 2841us + 2.02$	0.127	0.162
19f		Rm$_6$	$k_{600} = 929(us)^{0.75}Q^{0.011}$	0.102	0.160
19g		Rm$_7$	$k_{600} = 4725(us)^{0.86}Q^{-0.14}d^{0.66}$	0.128	0.287

[a]Average stream depth and flow velocity are taken from (Table 1). The average shear velocity, u_*, computed as $u_* = u(C_D)^{1/2}$, with C_D being the drag coefficient (Wüest and Lorke 2003). An average C_D of 3.3×10^{-3} was used for both sites based on further surveys of the River Avon sub-catchments (Rovelli et al. 2017). The average slope, 0.002 m m^{-1}, was estimated from GPS measurements during the respective field campaigns.

[b]Reference equation numbers and abbreviations from Aristegi et al. (2009) and Palumbo and Brown (2014), respectively.

[c]This equation requires depth in cm and flow velocity in cm s^{-1}.

[d]With k_2' being 31,183 s m^{-1} d^{-1} for $Q < 0.280$ m^3 s^{-1} and 22,500 s m^{-1} d^{-1} for $Q > 0.280$ m^3 s^{-1}, respectively (Palumbo and Brown 2014).

[e]These equations were identified to be the most suited (i.e., top performer) for the site mean depth and flow based on the suggestions of Palumbo and Brown (2014).

contrasts with the NR method, for instance, where estimates of k_2 obtained at night might not be applicable during the day. Furthermore, the OB approach relies on in situ measurements of local O₂ mass balance variables, rather than parametrizations and scaling relationship from literature values. The method is therefore ideal for investigating

discrepancies between the various procedures for estimating k_2 and thus strengthens the parameterization procedures applied for upscaling global estimates of outgassing coefficients for other gases such as CO_2 and CH_4.

In this study, the NR method systematically provided among the highest estimates of k_2 for both reaches. Values of k_{NR} were, on average, a factor of two higher than k_2 derived by the OB method (Fig. 5). The largest discrepancies, by up to a factor of three, were observed at nighttime, while, during the daytime, mean values were within reported uncertainties for this approach (Palumbo and Brown 2014). Potential issues with NR method applicability or dataset quality were deemed marginal, as both CE and GA met the requirements of the NR method (*see* "Methods" section), and the O_2 time series were of a high quality (Supporting Information Fig. S3). Therefore, the observed discrepancies in k_2 are attributed to a biased estimation of R derived at nighttime using the NR method (R_{NR}), leading to a systematic overestimation of k_2.

Studies investigating the effect of local inflows of O_2-depleted groundwater have shown that groundwater might bias the quantification of R in open water approaches and thus whole-stream O_2 budget assessments (e.g., McCutchan et al. 2002; Hall and Tank 2005; Koopmans and Berg 2015). The magnitude of such effect, which would lead to an overestimation of R, might vary according to hydrological characteristics and hydrological connectivity of each stream, ranging from negligible to substantial (*see* McCutchan et al. 2002). In this study, the contribution from groundwater to the O_2 budgets was quantified directly. At gaining reach GA, groundwater contributions to whole-stream estimates of R were limited to 0.5 mmol m^{-2} h^{-1}, representing < 5% of the mean R_{NR} (15.5 mmol m^{-2} h^{-1}); the combined R from the benthic compartment and water column activity was 6.7 mmol m^{-2} h^{-1}. At losing reach CE, contributions from groundwater were negligible but the NR method still estimated R at 8.7 mmol m^{-2} h^{-1}, which is some threefold higher than our direct measurements (2.8 mmol m^{-2} h^{-1}).

An overestimation of R during night could also result from a temporal misalignment between actual changes in whole stream respiration and physical parameters controlling gas exchange. As shown in both datasets (Figs. 2–3), temperature decreased at night until about 6–8 a.m., and directly affected the measured saturation deficit. If k_2 is assumed to be constant, as shown from our NR regression plots (*see* Supporting Information Fig. S3), then the temperature-driven increase in the O_2 concentration at saturation, and associated O_2 saturation deficit, will result in an erroneous estimate of the magnitude of R_{NR}.

It has recently been shown that k (and thus k_2) might display changes of up to a factor of 2–3 over timescales of 10 s of minutes to hours, even under constant hydrological conditions (e.g., Berg and Pace 2017), implying that k_2 will not remain constant over the several hours' time scale associated with the NR method. Since the NR approach considers changes in the magnitude of k_2 as a direct and instantaneous
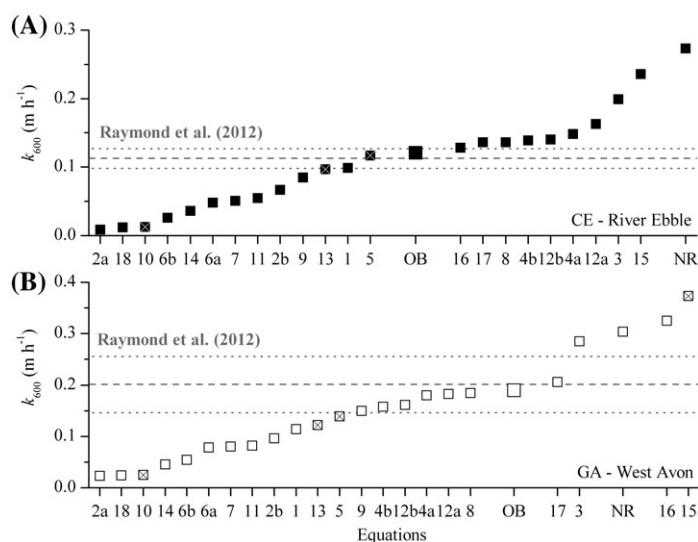
Fig. 5. Estimates of k_{600} (in m h^{-1}) for (**A**) River Ebble and (**B**) West Avon. Estimates are obtained from different published hydrological parameterizations (Eqs. 1–18, and Raymond et al. (2012)); from the O_2 budget (OB) method used in this study (*see* Eq. 4); and from the nighttime regression (NR) method. Equation numbering follows Table 4. Note that crossed equations were reported to be the "top-performer" within a specific mean depth and mean flow range from an extensive database of tracer-based k_2 values and hydrological parameters (*see* Palumbo and Brown 2014). Mean value and uncertainty range (dashed and dotted lines) for the hydrological parameterizations of Raymond et al. (2012) were obtained by combining mean and range of each equation (*see* Table 4; Supporting Information Fig. S6). Note that to better highlight the differences between the OB, NR and common parametrizations, the equation order was re-arranged to show an incremental increase in k_{600}.

consequence of changes in R, variability in k_2 could explain the magnitude of the R_{NR} bias obtained in this study, although the drivers of that variability, such as temperature, wind and stream discharge, need further investigation (Berg and Pace 2017).

Hydrological parameters such as stream depth, stream flow, and stream energy (e.g., slope, shear velocity) have been used to derive k_2 (e.g., O'Connor and Dobbins 1958; Palumbo and Brown 2014) and subsequently k_{600}. Given the local hydrology (0.4–0.57 m mean depth, 0.18–0.33 m s^{-1} mean flow velocity), our mean values of k_{600} derived with the (OB) method (0.121 ± 0.007 m h^{-1} for CE and 0.190 ± 0.016 m h^{-1} for GA), are well within the range predicted by 19 sets of proposed functional equations extracted from the literature (0.009–0.236 m h^{-1} at CE and 0.023–0.373 m h^{-1} at GA; Table 4; Fig. 5). NR-derived values were also within that range, although they ranked toward the upper end of the range. As expected from previous studies (*see* Aristegi et al. 2009; Palumbo and Brown 2014), estimates from each equation were highly scattered throughout the obtained range, with little consistency between the two sites. For instance, even equations that were previously identified to perform well in hydrology settings similar to our study, i.e., "top performer"

equations (*see* Palumbo and Brown 2014), still showed large discrepancies—both within and across sites (Fig. 5). In contrast, we found that the revised functional equations provided by Raymond et al. (2012) provided well-constrained estimates, which were not only consistent within sites (*see* Supporting Information Fig. S6), but also between sites, with mean k_{600} values (0.113 m h^{-1} for CE and 0.201 m h^{-1} for GA) within 5–7% of the local estimates from our OB method (Fig. 5).

Comments and recommendations

The aquatic eddy co-variance technique (AEC) has been shown to be an effective tool for quantifying streambed metabolism and, more recently, for the quantification of O_2 gas exchange and k from O_2 fluxes near the stream surface (Berg and Pace 2017). A combination of the AEC technique with other traditional methods appears to be a promising next step toward better constrained assessments of gas exchange and k dynamics in headwaters, provided that careful consideration is given to (1) the site selection and (2) the representativeness of the reach within the km-sized integration of, e.g., open-water approaches. The O_2 budget (OB) approach presented in this study serves as a proof-of-concept toward this goal. While the approach is more time consuming and field demanding than traditional methods, it does enable (1) the compartmentalization of stream metabolism and (2) the assessment of short-term k variability. The study has highlighted short-term variability in k dynamics with a dampened relationship to variations of well-known physical drivers. The apparent lack of correlation could be attributed to temporal misalignments between the variability of the derived k and physical drivers, and to small-scale variability in temperature. This was clearly observed at CE, where temperature-corrected k_{20} and k_{600} values still revealed a marked temperature dependency, suggesting that common temperature corrections were insufficient to fully account for the observed k variability. It remains unclear whether and to what extend such small-scale variability in temperature will affect the overall gas exchange.

Although the above aspects are still poorly constrained at the local scale and on short time scales (hours), estimates of k from the most recent functional parametrizations compared well with the independent assessments of this study and should therefore be preferred over earlier parametrizations. Validations of k on local scales such as the ones presented in this study are strongly required to strengthen and add more confidence to the upscaling of k for the quantification of large-scale metabolism and global emission of climate-relevant gases such as CO_2 and CH_4 across headwaters and throughout riverine networks.

References

Appling, A. P., R. O. Hall, C. B. Yackulic, and M. Arroita. 2018. Overcoming equifinality: Leveraging long time series for stream metabolism estimation. J. Geophys. Res. Biogeosci. **123**: 624–645. doi:10.1002/2017JG004140

Aristegi, L., O. Izagirre, and A. Elosegi. 2009. Comparison of several methods to calculate reaeration in streams, and their effects on estimation of metabolism. Hydrobiologia **635**: 113–124. doi:10.1007/S10750-009-9904-8

Attard, K. M., R. N. Glud, D. F. McGinnis, and S. Rysgaard. 2014. Seasonal rates of benthic primary production in a Greenland fjord measured by aquatic eddy-correlation. Limnol. Oceanogr. **59**: 1555–1569. doi:10.4319/lo.2014.59.5.1555

Aufdenkampe, A. K., E. Mayorga, P. A. Raymond, J. M. Melack, S. C. Doney, S. R. Alin, R. E. Aalto, and K. Yoo. 2011. Riverine coupling of biogeochemical cycles between land, oceans, and atmosphere. Front. Ecol. Environ. **9**: 53–60. doi:10.1890/100014

Bansal, M. K. 1973. Atmospheric reaeration in natural streams. Water Res. **7**: 769–782. doi:10.1016/0043-1354(73)90092-4

Battin, T. J., L. A. Kaplan, S. Findlay, C. S. Hopkinson, E. Marti, A. I. Packman, J. D. Newbold, and F. Sabater. 2008. Biophysical controls on organic carbon fluxes in fluvial networks. Nat. Geosci. **1**: 95–100. doi:10.1038/Ngeo101

Bennett, J. P., and R. E. Rathbun. 1972. Reaeration in open-channel flow. U.S. Geological Survey Prof. Pap. 737, U.S. Government Printing Office, Washington, DC. Available from: https://pubs.usgs.gov/pp/0737/report.pdf

Benson, A., and others. 2014. Quantifying reaeration rates in alpine streams using deliberate gas tracer experiments. Water **6**: 1013–1027. doi:10.3390/w6041013

Berg, P., H. Røy, F. Janssen, V. Meyer, B. B. Jørgensen, M. Huettel, and D. de Beer. 2003. Oxygen uptake by aquatic sediments measured with a novel non-invasive eddy-correlation technique. Mar. Ecol. Prog. Ser. **261**: 75–83. doi:10.3354/meps261075

Berg, P., H. Røy, and P. L. Wiberg. 2007. Eddy correlation flux measurements: The sediment surface area that contributes to the flux. Limnol. Oceanogr. **52**: 1672–1684. doi:10.4319/lo.2007.52.4.1672

Berg, P., M. L. Delgard, R. N. Glud, M. Huettel, C. E. Reimers, and M. L. Pace. 2017. Non-invasive flux measurements at the benthic interface: The aquatic eddy covariance technique. Limnol. Oceanogr. **7**: 1–50. doi:10.1002/loe2.10005

Berg, P., and M. L. Pace. 2017. Continuous measurement of air-water gas exchange by underwater eddy covariance. Biogeosciences **14**: 5595–5606. doi:10.5194/bg-14-5595-2017

Binley, A., S. Ullah, A. L. Heathwaite, C. Heppell, P. Byrne, K. Lansdown, M. Trimmer, and H. Zhang. 2013. Revealing the spatial variability of water fluxes at the groundwater-surface water interface. Water Resour. Res. **49**: 3978–3992. doi:10.1002/wrcr.20214

Butman, D., and P. A. Raymond. 2011. Significant efflux of carbon dioxide from streams and rivers in the United States. Nat. Geosci. **4**: 839–842. doi:10.1038/ngeo1294

Cadwallader, T. E., and A. J. McDonnell. 1969. A multivariate analysis of reaeration data. Water Res. **3**: 731–742. doi:10.1016/0043-1354(69)90037-2

Chapra, S. C., and D. M. DiToro. 1991. Delta method for estimating primary production, respiration, and reaeration in streams. J. Environ. Eng. **117**: 640–655. doi:10.1061/(ASCE)0733-9372(1991)117:5(640

Churchill, M. A., H. L. Elmore, and R. A. Buckingham. 1962. The prediction of stream reaeration rates. Int. J. Air Water Pollut. **6**: 467–467. doi:10.1016/B978-1-4832-8391-3.50015-4

Cole, J. J., and others. 2007. Plumbing the global carbon cycle: Integrating inland waters into the terrestrial carbon budget. Ecosystems **10**: 172–184. doi:10.1007/s10021-006-9013-8

Correa-Gonzalez, J. C., M. D. Chavez-Parga, J. A. Cortes, and R. M. Perez-Munguia. 2014. Photosynthesis, respiration and reaeration in a stream with complex dissolved oxygen pattern and temperature dependence. Ecol. Model. **273**: 220–227. doi:10.1016/j.ecolmodel.2013.11.018

Crawford, J. T., and E. H. Stanley. 2016. Controls on methane concentrations and fluxes in streams draining human-dominated landscapes. Ecol. Appl. **26**: 1581–1591. doi:10.1890/15-1330

Demars, B. O. L., and J. R. Manson. 2013. Temperature dependence of stream aeration coefficients and the effect of water turbulence: A critical review. Water Res. **47**: 1–15. doi:10.1016/j.watres.2012.09.054

Demars, B. O. L., J. Thompson, and J. R. Manson. 2015. Stream metabolism and the open diel oxygen method: Principles, practice, and perspectives. Limnol. Oceanogr.: Methods **13**: 356–374. doi:10.1002/lom3.10030

Dobbins, W. E. 1965. BOD and oxygen relationships in streams. J. Sanit. Eng. Div. **90**: 53–78.

Donis, D., and others. 2015. An assessment of the precision and confidence of aquatic Eddy correlation measurements. J. Atmos. Oceanic Technol. **32**: 642–655. doi:10.1175/JTECH-D-14-00089.1

Downing, J. A., and others. 2012. Global abundance and size distribution of streams and rivers. Inland Waters **2**: 229–236. doi:10.5268/Iw-2.4.502

Elmore, H. L., and W. F. West. 1961. Effect of water temperature on stream reaeration. J. Sanit. Eng. Div. Am. Soc. Civ. Eng. **87**: 59–71.

Garcia, H. E., and L. I. Gordon. 1992. Oxygen solubility in seawater—better fitting equations. Limnol. Oceanogr. **37**: 1307–1312. doi:10.4319/lo.1992.37.6.1307

Genereux, D. P., and H. F. Hemond. 1992. Determination of gas exchange rate constants for a small stream on Walker Branch watershed, Tennessee. Water Resour. Res. **28**: 2365–2374. doi:10.1029/92WR01083

Grace, M. R., and S. J. Imberger. 2006. Stream metabolism: Performing and interpreting measurements, p. 204. Water Studies Centre, Monash Univ. Report for the Murray Darling Basin Commission and the New South Wales Department of Environment and Climate Change.

Grace, M. R., D. P. Giling, S. Hladyz, V. Caron, R. M. Thompson, and R. Mac Nally. 2015. Fast processing of diel oxygen curves: Estimating stream metabolism with BASE

(BAyesian single-station estimation). Limnol. Oceanogr.: Methods **13**: 103–114. doi:10.1002/lom.10011

Gundersen, J. K., N. B. Ramsing, and R. N. Glud. 1998. Predicting the signal of O₂ microsensors from physical dimensions, temperature, salinity, and O₂ concentration. Limnol. Oceanogr. **43**: 1932–1937. doi:10.4319/lo.1998.43.8.1932

Hall, R. O., and J. L. Tank. 2005. Correcting whole-stream estimates of metabolism for groundwater input. Limnol. Oceanogr.: Methods **3**: 222–229. doi:10.4319/lom.2005.3.222

Hall, R. O., T. A. Kennedy, and E. J. Rosi-Marshall. 2012. Air-water oxygen exchange in a large whitewater river. Limnol. Oceanogr.: Fluids and Environments **2**: 1–11. doi:10.1215/21573689-1572535

Heppell, C. M., and A. Binley. 2016a. Hampshire Avon: Daily discharge, stage and water chemistry data from four tributaries (Sem, Nadder, West Avon, Ebble). NERC Environmental Information Data Centre. doi:10.5285/0dd10858-7b96-41f1-8db5-e7b4c4168af5

Heppell, C. M., and A. Binley. 2016b. Vertical head gradient, saturated hydraulic conductivity and pore water chemistry data from six river reaches. NERC Environmental Information Data Centre. doi:10.5285/d82a04ce-f04d-40b4-9750-1a2bf7dc29a3

Heppell, C. M., and others. 2017. Hydrological controls on DOC: Nitrate resource stoichiometry in a lowland, agricultural catchment, southern UK. Hydrol. Earth Syst. Sci. **21**: 4785–4802. doi:10.5194/hess-21-4785-2017

Holtappels, M., R. N. Glud, D. Donis, B. Liu, A. Hume, F. Wenzhöfer, and M. M. M. Kuypers. 2013. Effects of transient bottom water currents and oxygen concentrations on benthic exchange rates as assessed by eddy correlation measurements. J. Geophys. Res.: Oceans **118**: 1157–1169. doi:10.1002/jgrc.20112

Holtgrieve, G. W., D. E. Schindler, T. A. Branch, and Z. T. A'mar. 2010. Simultaneous quantification of aquatic ecosystem metabolism and reaeration using a Bayesian statistical model of oxygen dynamics. Limnol. Oceanogr. **55**: 1047–1063. doi:10.4319/lo.2010.55.3.1047

Hornberger, G. M., and M. G. Kelly. 1975. Atmospheric reaeration in a river using productivity analysis. J. Environ. Eng. Div. **101**: 729–739.

Hotchkiss, E. R., R. O. Hall, R. A. Sponseller, D. Butman, J. Klaminder, H. Laudon, M. Rosvall, and J. Karlsson. 2015. Sources of and processes controlling CO₂ emissions change with the size of streams and rivers. Nat. Geosci. **8**: 696–699. doi:10.1038/ngeo2507

Isaacs, W. P., and A. F. Gaudy. 1968. Atmospheric oxygenation in a simulated stream. J. Sanit. Eng. Div. **94**: 319–344.

Jahne, B., K. O. Munnich, R. Bosinger, A. Dutzi, and W. Huber. 1987. On parameters influencing air-water gas exchange. J. Geophys. Res. **74**: 456–464. doi:10.1029/JC092iC02p01937

Kilpatrick, F. A., R. E. Rathbun, N. Yotsukura, G. W. Parker, and L. L. DeLong. 1989. Determination of stream reaeration coefficients by use of tracers. Page 52 Techniques of water-resources investigations 3-A18. U.S. Geological Survey, Denver, Colorado.

Koopmans, D., and P. Berg. 2015. Stream oxygen flux and metabolism determined with the open water and eddy correlation techniques. Limnol. Oceanogr. **60**: 1344–1355. doi:10.1002/lno.10103

Krenkel, P. A., and G. T. Orlob. 1963. Turbulent diffusion and the reaeration coefficient. J. Sanit. Eng. Div. **88**: 53–83.

Langbein, W. B., and W. H. Durum. 1967. The aeration capacity of streams. USGS Circ. S42, USGS, Washington, DC.

Long, M. H., and D. P. Nicholson. 2018. Surface gas exchange determined from an aquatic eddy covariance floating platform. Limnol. Oceanogr.: Methods **16**: 145–159. doi:10.1002/lom3.10233

Marx, A., J. Dusek, J. Jankovec, M. Sanda, T. Vogel, R. van Geldern, J. Hartmann, and J. A. C. Barth. 2017. A review of CO$_2$ and associated carbon dynamics in headwater streams: A global perspective. Rev. Geophys. **55**: 560–585. doi:10.1002/2016RG000547

Marzolf, E. R., P. J. Mulholland, and A. D. Steinman. 1994. Improvements to the diurnal upstream-downstream dissolved-oxygen change technique for determining whole-stream metabolism in small streams. Can. J. Fish. Aquat. Sci. **51**: 1591–1599. doi:10.1139/F94-158

McBride, G. B., and S. C. Chapra. 2005. Rapid calculation of oxygen in streams: Approximate delta method. J. Environ. Eng. **131**: 336–342. doi:10.1061/(ASCE)0733-9372(2005)131:3(336

McCutchan, J. H., J. F. Saunders, W. M. Lewis, and M. G. Hayden. 2002. Effects of groundwater flux on open-channel estimates of stream metabolism. Limnol. Oceanogr. **47**: 321–324. doi:10.4319/lo.2002.47.1.0321

McGinnis, D. F., P. Berg, A. Brand, C. Lorrai, T. J. Edmonds, and A. Wüest. 2008. Measurements of eddy correlation oxygen fluxes in shallow freshwaters: Towards routine applications and analysis. Geophys. Res. Lett. **35**: L04403. doi:10.1029/2007GL032747

McGinnis, D. F., S. Cherednichenko, S. Sommer, P. Berg, L. Rovelli, R. Schwarz, R. N. Glud, and P. Linke. 2011. Simple, robust eddy correlation amplifier for aquatic dissolved oxygen and hydrogen sulfide flux measurements. Limnol. Oceanogr.: Methods **9**: 340–347. doi:10.4319/lom.2011.9.340

McGinnis, D. F., S. Sommer, A. Lorke, R. N. Glud, and P. Linke. 2014. Quantifying tidally driven benthic oxygen exchange across permeable sediments: An aquatic eddy correlation study. J. Geophys. Res. Oceans **119**: 6918–6932. doi:10.1002/2014JC010303

Moog, D. B., and G. H. Jirka. 1998. Analysis of reaeration equations using mean multiplicative error. J. Environ. Eng. **124**: 104–110. doi:10.1061/(ASCE)0733-9372(1998)124:2(104)

Mori, N., T. Suzuki, and S. Kakuno. 2007. Noise of acoustic Doppler velocimeter data in bubbly flow. J. Eng. Mech. **133**: 122–125. doi:10.1061/(ASCE)0733-9399(2007)133:1(122

Mulholland, P. J., and others. 2001. Inter-biome comparison of factors controlling stream metabolism. Freshw. Biol. **46**: 1503–1517. doi:10.1046/j.1365-2427.2001.00773.x

Negulescu, M., and V. Rojanski. 1969. Recent research to determine reaeration coefficient. Water Res. **3**: 189–192. doi:10.1016/0043-1354(69)90058-X

Nightingale, P. D., G. Malin, C. S. Law, A. J. Watson, P. S. Liss, M. I. Liddicoat, J. Boutin, and R. C. Upstill-Goddard. 2000. In situ evaluation of air-sea gas exchange parameterizations using novel conservative and volatile tracers. Global Biogeochem. Cycles **14**: 373–387. doi:10.1029/1999gb900091

O'Connor, D. J., and W. E. Dobbins. 1958. Mechanism of reaeration in natural streams. Am. Soc. Civ. Eng. **123**: 641–684.

Odum, H. T. 1956. Primary production in flowing waters. Limnol. Oceanogr. **1**: 102–117. doi:10.4319/lo.1956.1.2.0102

Owens, M. 1974. Measurement on non-isolated natural communities in running waters. *In* R. A. Vollenweider [ed.], A manual on methods for measuring primary production in aquatic environments. Blackwell Scientific.

Owens, M., R. W. Edwards, and J. W. Gibbs. 1964. Some reaeration studies in streams. Int. J. Air Water Pollut. **8**: 469–486.

Padden, T. J., and E. F. Gloyna. 1971. Simulation of stream processes in a model river. Rep. No. EHE-70-23, Univ. of Texas, Austin, TX.

Palumbo, J. E., and L. C. Brown. 2014. Assessing the performance of reaeration prediction equations. J. Environ. Eng. **140**: 04013013. doi:10.1061/(ASCE)EE.1943-7870.0000799

Parker, G. W., and F. B. Gay. 1987. A procedure for estimating reaeration coefficients for Massachusetts streams. U.S. Geological Survey. Water Resources Invest. Rep. 86-4111. USGS, Reston, VA.

Parker, G. W., and L. A. DeSimone. 1992. Estimating reaeration coefficients for low-slope streams in Massachusetts and New York, 1985–88. U.S. Geological Survey, Water Resources Invest. Rep. 91-4188, USGS, Washington, DC.

Parkhurst, J. D., and R. D. Pomeroy. 1972. Oxygen absorption in streams. J. Sanit. Eng. Div. **98**: 101–124.

Raymond, P. A., and others. 2012. Scaling the gas transfer velocity and hydraulic geometry in streams and small rivers. Limnol. Oceanogr.: Fluids and Environments **2**: 41–53. doi:10.1215/21573689-1597669

Raymond, P. A., and others. 2013. Global carbon dioxide emissions from inland waters. Nature **503**: 355–359. doi:10.1038/nature12760

Reid, S. E., P. A. Mackinnon, and T. Elliot. 2007. Direct measurements of reaeration rates using noble gas tracers in the River Lagan, Northern Ireland. Water Environ. J. **21**: 182–191. doi:10.1111/j.1747-6593.2007.00069.x

Revsbech, N. P. 1989. An oxygen microelectrode with a guard cathode. Limnol. Oceanogr. **34**: 474–478. doi:10.4319/lo.1989.34.2.0474

Rheuban, J. E., P. Berg, and K. J. McGlathery. 2014. Multiple timescale processes drive ecosystem metabolism in eelgrass (*Zostera marina*) meadows. Mar. Ecol. Prog. Ser. **507**: 1–13. doi:10.3354/Meps10843

Riley, A. J., and W. K. Dodds. 2013. Whole-stream metabolism: Strategies for measuring and modeling diel trends of dissolved oxygen. Freshw. Sci. **32**: 56–69. doi:10.1899/12-058.1

Rovelli, L., K. M. Attard, H. Stahl, and R. N. Glud. 2016a Flow velocity transects collected seasonally at six tributaries of Hampshire River Avon from 2013 to 2014. NERC Environmental Information Data Centre. doi:10.5285/16df35a9-90ab-4273-8b6c-5ef3648ec76d

Rovelli, L., K. M. Attard, H. Stahl, and R. N. Glud. 2016b. In situ near-streambed light regime and water column dissolved oxygen and temperature measurements performed seasonally at six tributaries of Hampshire River Avon from 2013 to 2014. NERC Environmental Information Data Centre. doi:10.5285/c1f14c54-ffe1-4581-b479-897ff9262e98

Rovelli, L., K. M. Attard, A. Binley, C. M. Heppell, H. Stahl, M. Trimmer, and R. N. Glud. 2017. Reach-scale river metabolism across contrasting sub-catchment geologies: Effect of light and hydrology. Limnol. Oceanogr. **62**: S381–S399. doi:10.1002/lno.10619

Siders, A. C., D. M. Larson, J. Ruegg, and W. K. Dodds. 2017. Probing whole-stream metabolism: Influence of spatial heterogeneity on rate estimates. Freshw. Biol. **62**: 711–723. doi:10.1111/fwb.12896

Smoot, J. L. 1988. An examination of stream reaeration coefficients and hydraulic conditions in a pool-and-riffle stream. Ph.D. Dissertation, Virginia Polytechnic Institute and State Univ..

Stanley, E. H., N. J. Casson, S. T. Christel, J. T. Crawford, L. C. Loken, and S. K. Oliver. 2015. The ecology of methane in streams and rivers: Patterns, controls, and global significance. Ecol. Monogr. **86**: 146–171. doi:10.1890/15-1027.1

Sweeney, C., E. Gloor, A. R. Jacobson, R. M. Key, G. McKinley, J. L. Sarmiento, and R. Wanninkhof. 2007. Constraining global air-sea gas exchange for CO₂ with recent bomb ¹⁴C measurements. Global Biogeochem. Cycles **21**: Gb2015. doi:10.1029/2006gb002784

Thackston, E. L., and P. A. Krenkel. 1969. Reaeration prediction in natural streams. J. Sanit. Eng. Div. **95**: 65–94.

Thackston, E. L., and J. W. Dawson. 2001. Recalibration of a reaeration equation. J. Environ. Eng. **127**: 317–321. doi:10.1061/(ASCE)0733-9372(2001)127:4(317

Tobias, C. R., J. K. Bohlke, J. W. Harvey, and E. Busenberg. 2009. A simple technique for continuous measurement of time-variable gas transfer in surface waters. Limnol. Oceanogr.: Methods **7**: 185–195. doi:10.4319/lom.2009.7

Tranvik, L. J., and others. 2009. Lakes and reservoirs as regulators of carbon cycling and climate. Limnol. Oceanogr. **54**: 2298–2314. doi:10.4319/lo.2009.54.6_part_2.2298

Trimmer, M., J. Grey, C. M. Heppell, A. G. Hildrew, K. Lansdown, H. Stahl, and G. Yvon-Durocher. 2012. River bed carbon and nitrogen cycling: State of play and some new directions. Sci. Total Environ. **434**: 143–158. doi:10.1016/j.scitotenv.2011.10.074

Tsivoglou, E. C., and L. A. Neal. 1976. Tracer measurement of reaeration: 3. Predicting the reaeration capacity of inland streams. J. Water Pollut. Control Fed **48**: 2669–2689.

Wanninkhof, R. 1992. Relationship between wind speed and gas exchange over the ocean. J. Geophys. Res. **97**: 7373–7382. doi:10.1029/92JC00188

Wanninkhof, R. 2014. Relationship between wind speed and gas exchange over the ocean revisited. Limnol. Oceanogr.: Methods **12**: 351–362. doi:10.4319/lom.2014.12.351

Wanninkhof, R., P. J. Mulholland, and J. W. Elwood. 1990. Gas exchange rates for a first-order stream determined with deliberate and natural tracers. Water Resour. Res. **26**: 1621–1630. doi:10.1029/WR026i007p01621

Watson, D. 1987. Hydraulic effects of aquatic weeds in U.K. rivers. Regul. Rivers Res. Manage. **1**: 211–227. doi:10.1002/rrr.3450010303

Winkler, L. 1888. Die Bestimmung des in Wasser gelösten Sauerstoffes. Ber. Dtsch. Chem. Ges. **21**: 2843–2855. doi:10.1002/cber.188802102122

Wüest, A., and A. Lorke. 2003. Small-scale hydrodynamics in lakes. Annu. Rev. Fluid Mech. **35**: 373–412. doi:10.1146/annurev.fluid.35.101101.161220

Conflict of Interest
None declared.